Journal of Hazardous Materials 185 (2011) 598–605

Contents lists available at ScienceDirect

Journal of Hazardous Materials

journal homepage: www.elsevier.com/locate/jhazmat

Rheological characterization of xanthan suspensions of nanoscale iron for injection in porous media

Silvia Comba [a], Davide Dalmazzo [b], Ezio Santagata [b], Rajandrea Sethi [a,*]

[a] DITAG - Dipartimento di Ingegneria del Territorio, dell'Ambiente e delle Geotecnologie, Politecnico di Torino, Torino, Italy
[b] DITIC - Dipartimento di Idraulica, Trasporti ed Infrastrutture Civili, Politecnico di Torino, Torino, Italy

ARTICLE INFO

Article history:
Received 11 February 2010
Received in revised form
18 September 2010
Accepted 20 September 2010
Available online 25 September 2010

Keywords:
Xanthan
Nanoscale zerovalent iron (NZVI)
Contaminated aquifer
Rheology
Porous media
Gel network

ABSTRACT

Nanoscale zerovalent iron (NZVI) represents one of the most interesting reagents for the remediation of contaminated aquifers, but its application is hindered by a lack of colloidal stability. Prior studies have shown that nanoscale iron slurries can be successfully stabilized against aggregation and sedimentation through dispersion in xanthan solutions; thus, further research was carried out by focusing on the flow behavior of xanthan-modified NVZI suspensions.

This work aims at understanding the rheological properties of NZVI-xanthan suspensions, which have been extensively tested under two different flow conditions: simple shear flow and flow through a porous medium. According to both experimental approaches, the suspensions show a shear thinning behavior that is dependent on iron concentration. These rheological properties are explained by referring to the microstructure of the colloidal system. Flow equations have been formulated and solved in radial coordinates in order to demonstrate the feasibility of such suspensions in field scale applications.

1. Introduction

Granular zerovalent iron has been widely used in permeable reactive barriers to effectively remove a variety of common environmental contaminants, including heavy metals, pesticides, chlorinated organic solvents, volatile organic compounds (VOCs) [1–6].

Nanoscale zerovalent iron (NZVI) is characterized by a superior reactivity if compared with granular iron and can be injected in the subsurface more easily [7]. The diffusion of NZVI technology is hindered by a lack of colloidal stability of the injection fluid and by the consequent limited delivery of nanoscale particles which results from the filtration process through porous media. Thus, as documented in literature, several researchers have devoted their efforts to the identification of suitable agents that can improve suspension stability and mobility. A wide range of additives has been tested including polyacrylate [8–10], triblock copolymers [11,12], polyvinyl alcohol-co-vinyl acetate-co-itaconic [13], guar gum [14] and [15], carboxymethyl cellulose [16,17], starch [18], poly(4-styrenesulfonate) [18], polyelectrolyte mixtures [19] and xanthan gum [20] and [21]. The latter biopolymer – xanthan gum – appears to be especially attractive not only for its environmental-friendly nature, but also since it has proved to be an effective stabilizing agent for highly concentrated iron suspensions that are required in field applications [20]. Even though preliminary results are encouraging [20] and [21], several issues still have to be addressed in order to fully support the use of xanthan-modified NVZI suspensions. In particular, a direct evaluation of the flow behavior through porous media is essential in order to assess the effectiveness of particle delivery which results from fluid injection. Moreover, rheological properties need to be thoroughly investigated since they can have an important impact on field scale implementation projects, where pressure should not exceed the instrumental limit of pumping devices and soil fracturing limit.

The flow of xanthan gum solutions and of other polymeric fluids has been widely investigated due to their relevance in the fields of chemical, environmental and petroleum engineering fields [22–26]. Previous research has shown that the bulk rheology of xanthan is characterized by weak gel properties at low shear rates, which are attributed to polymer entanglement. However, such a structure is progressively broken down by the application of higher shear rates, which results in strong shear thinning behavior [27–30].

Given that the internal geometry of the pore space in either a packed bed or a porous matrix is rather complex, phenomena which occur during filtration are significantly different from those

* Corresponding author at: DITAG - Politecnico di Torino - Corso Duca degli Abruzzi, 24 - 10129 Torino, Italy. Tel.: +39 011 090 7735; fax: +39 011 090 7699.
E-mail addresses: silvia.comba@polito.it (S. Comba), rajandrea.sethi@polito.it (R. Sethi).

0304-3894/$ – see front matter © 2010 Elsevier B.V. All rights reserved.
doi:10.1016/j.jhazmat.2010.09.060

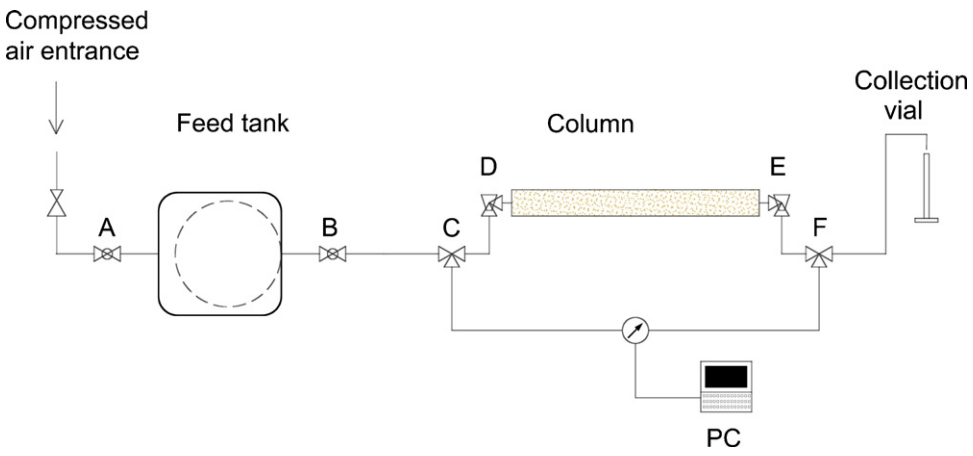

Fig. 1. Experimental set up for porous media experiments.

described by any simple rheometric flow [23]. For example, flow within porous media has an extensional component, especially at high shear rates, which causes an increase in the apparent viscosity of xanthan solutions [31]. Another consequence of the complexity of porous media structure is the difficulty in predicting the flow behavior of viscous and viscoelastic fluids. Chhabra et al. [32] provided a detailed review of the different techniques to predict the frictional pressure loss for viscous and viscoelastic fluids through packed beds, namely: capillary bundle model, submerged object model (drag theories), averaging methods [33,34] and empirical dimensionless correlations.

Many researchers have actually chosen an empirical approach and derived an "in situ" or "apparent" viscosity, which is an average property arising from upscaling of point wise shear rate at the microscale [31,35–38]. According to this approach, under laminar flow, the apparent viscosity μ_{app} is defined on the basis of Darcy's law:

$$\mu_{app} = \frac{k}{q} \cdot \frac{\Delta P}{L} \quad (1)$$

where ΔP is the pressure drop over a length L of a porous medium, q is specific discharge, k is the permeability. The effective shear rate within the porous medium is defined according to the following expression [36]:

$$\dot{\gamma}_{pm} = \frac{q}{\sqrt{k \cdot n_e}} \quad (2)$$

where n_e is the effective porosity of the medium.

Experimental results indicate that viscosity versus shear rate curves obtained from experiments in porous media interpreted according to the above given equations have the same shape of those which are derived from classical rheological tests. Moreover, curves can be superimposed by multiplying the shear rate by a shift factor α [36,39] (i.e. it is an adjustable parameter). The shift factor, α, is a function of both the bulk rheology and the pore structure [35] and its value generally lies in the range 1–15 [35].

This work aims at understanding the rheological properties of nanoscale iron–xanthan suspensions, which were extensively tested under two different flow conditions: simple shear flow and flow through porous medium. The observed rheological properties are explained by referring to the microstructure of the colloidal system. The implications of the rheological behavior of the suspensions in full scale applications are be also discussed.

2. Experimental

2.1. Materials

Reactive nanoscale zerovalent iron (NZVI) was obtained from Toda Kyogo Corp. The nanoscale particles are composed of a Fe^0 core enclosed in a Fe_3O_4 shell which is covered by a small amount of polymaleic polymer in order to provide electrosteric stabilization [40]. The material was provided in the form of a concentrated water slurry (200 g l^{-1}).

Xanthan gum was supplied by Jungbunzlauer, Switzerland, in the form of a powder.

Xanthan solutions were prepared by dispersing the required amount of solid polymer in deionized water and by thereafter subjecting the system to thorough stirring.

NZVI-xanthan dispersions were prepared by following a two step procedure. At first the concentrated as received-slurry was added to water and the resulting suspension was ultrasonicated and mixed using a high shear rotor-stator processor for 20 min utilizing an in line system (in order to break iron aggregates present in the iron slurry). In the second step of the procedure, a concentrated xanthan gel (20 g l^{-1} xanthan) was added to the suspension with the dosage required to reach target NVZI and xanthan concentrations [20]. Resulting NZVI-xanthan suspensions considered in the investigation were characterized by a final xanthan concentration of 3 g l^{-1}, whereas the iron concentration ranged from 5 to 30 g l^{-1}.

2.2. Equipment and procedures

Bulk rheological characterization of the xanthan solutions and NZVI-xanthan suspensions was performed by means of a dynamic shear rheometer (Anton Paar Physica MCR 301) equipped with coaxial cylinders (1.13 mm gap). For the region of shear rates from 1.5×10^3 to 10^5 s^{-1}, parallel plate geometry with a gap of 0.1 mm was used. This region of very high shear rates, was investigated only for the xanthan solutions, because iron particles in the suspensions would have damaged the instrument at very small gaps.

The rheological properties inside the porous medium were studied using an experimental set up consisting of a pressurized feed tank connected to a 1.8 cm diameter column filled with silica sand (Fig. 1). The pressurized feed tank was used to inject the suspensions into the column. A rubber flask was used to prevent air dissolution in the liquid suspensions. Pressure was controlled by a valve, located between the tank and the entrance to the column, while pressure drop across the column was measured continuously by means of differential pressure meters (PCE-Instruments) connected to a PC. The operation range of the pressure transducers is

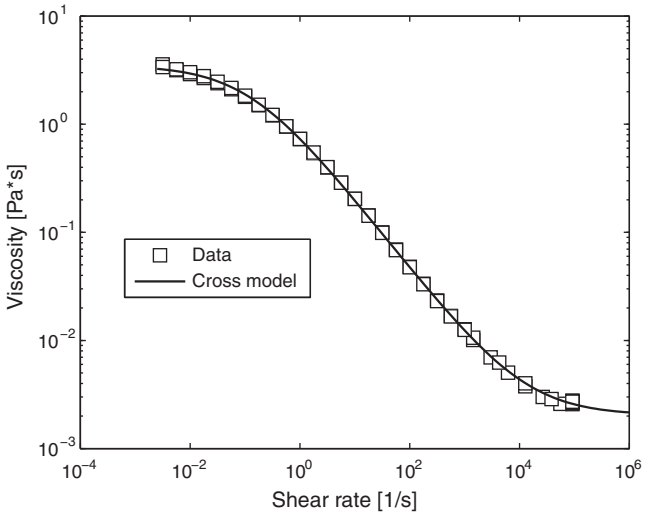

Fig. 2. Simple shear rheology of a xanthan solutions as a function of the shear rate: experimental data (symbols) and fitting with cross equation (solid line).

respectively 0 to ±350 mbar, 0 to ±2000 mbar and 0 to ±6900 mbar. The porous medium consisted of a column filled with silica sand (SiO_2-95%), characterized by a grain size comprised between 0.5 and 1.0 mm. Columns were packed to an average effective porosity of 49%, measured as the weight difference between saturated and dry sand. An average permeability of 1.1×10^{-9} m^2 (standard deviation of 6×10^{-11} m^2) was determined from triplicate flow experiments using water.

An injection test was conducted to evaluate the ability of xanthan gum to carry iron particles through porous media. The experiment took place in a 1 m length column (diameter 2.5 cm), using a 20 g l^{-1} iron concentration dispersed in a 3 g l^{-1} xanthan solution. During the experiment, 4 pore volumes of NZVI-xanthan suspensions were injected into the column, which had previously been flushed with water, at a pressure of 4 bar. The breakthrough iron concentration was measured by means of magnetic susceptibility measurements as described in Ref. [21].

Experiments designed to evaluate the rheological behavior of suspensions during their flow through the porous medium were performed in reduced length columns (30 cm) to minimize filtration effects. Columns were preliminary saturated with the tested suspensions during packing, in order to enhance a homogeneous distribution along the column. After pressurizing the feed reservoir, the valve was slowly opened until the desired flow rate was reached, and the consequent discharge (Q) and pressure drop along the column (ΔP) were measured.

Apparent viscosity μ_{app} was calculated from pressure drop and the discharge as previously described in Eq. (1), while the shear rate $\dot{\gamma}_{pm}$ experienced by the material in the porous media was calculated according to Eq. (2).

3. Results

3.1. Injection test

Iron concentration measured at the outlet of the column during the injection test reached an asymptotic value of more than 90% of the in-flow value.

3.2. Rheology

3.2.1. Bulk rheology

Fig. 2 shows the viscosity of the xanthan solutions as a function of shear rate. Viscosity is almost constant at low shear rates, while shear thinning behavior can be observed at higher shear rates. Finally viscosity becomes constant again at higher shear rates.

Table 1
Coefficient of the Cross model, determined through non linear regression, for a xanthan solution at 3 g l^{-1} and for the same solution at different iron concentrations.

	Xanthan	Iron (5 g l^{-1})	Iron (17.5 g l^{-1})	Iron (30 g l^{-1})
μ	3.51	1.02	2.32	4.09
μ_∞	0.0020	0.0020	0.0020	0.0020
λ	7.89	2.46	6.78	9.26
m	0.65	0.60	0.63	0.69

The observed remarkable shear-dependent behavior can be explained in terms of the progressive destruction of intermolecular low-energy bonds established through polysaccharide chains [41]. This behavior is typical of structured fluids or weak gels, where polymer concentrations are high and the coils are packed [42].

The shear rate that divides the first Newtonian region from the shear thinning region, which is defined as "critical shear rate" ($\dot{\gamma}_c$) is very low in the case of xanthan (about 10^{-2} s^{-1}) and this phenomenon was attributed to the propensity of the molecules to be oriented under shear on account of their extended and semi-rigid conformation [43]. In addition to xanthan solutions, many pure liquids, dilute polymer solutions and suspensions display Newtonian viscosity at high shear rates [44,45].

The overall rheological behavior can be described using the Cross model [46]:

$$\mu = \frac{\mu_0 - \mu_\infty}{1 + (\lambda\dot{\gamma})^m} + \mu_\infty \quad (3)$$

where μ_0 and μ_∞ are the asymptotic values of viscosity at low and very high shear rates, m measures the degree of dependence of viscosity on the shear rate in the shear-thinning region, while λ is related to the shear rate value where shear thinning behavior starts.

The Cross model fitting of the experimental data is reported in Fig. 2, while Table 1 shows the coefficients determined through non-linear minimization using the Newton algorithm. The ratio of the standard deviation of the fitting parameters and the average value of the parameter is below 6%. The value of viscosity at high shear rates, μ_∞, was estimated to be equal to 0.002 Pa s. This value is close to the one reported by [47] (0.001 Pa s for a 5 g l^{-1} xanthan solution) and to the one reported by [48] (0.01 Pa s for a 10/20 g l^{-1} xanthan solutions).

NZVI-xanthan suspensions display a rheological behavior which is similar to that of xanthan solutions (Fig. 3). However, some particular features, connected to the presence of NZVI, are also worth mentioning. First the value of viscosity in NZVI suspensions increases with increasing particle volume fractions. Second, as the concentration increases, shear-thinning behavior begins at progressively lower shear rates. From a comparison with the xanthan solutions, it emerges that the presence of small amounts of iron particles reduces the viscosity of the system, while the viscosity is more similar to that of pure xanthan at higher iron concentrations.

The Cross model was used to describe the NZVI-xanthan system. The μ_∞ was set equal to the μ_∞ of the liquid medium, since according to the plot in Fig. 3, both xanthan solution and NZVI-xanthan suspensions converge from about 100 s^{-1} onwards, and since all materials, even water, displays a certain viscosity value at high shear rates [45].

The fitted experimental data are shown in Fig. 4, while Table 1 reports the coefficients of the Cross model determined through non-linear minimization using the Newton algorithm. The ratio of the standard deviation of the fitting parameters and the average value of the parameter is below 6%. As shown in Table 1, μ_0, λ and m increase for increasing iron concentrations, which indicates that

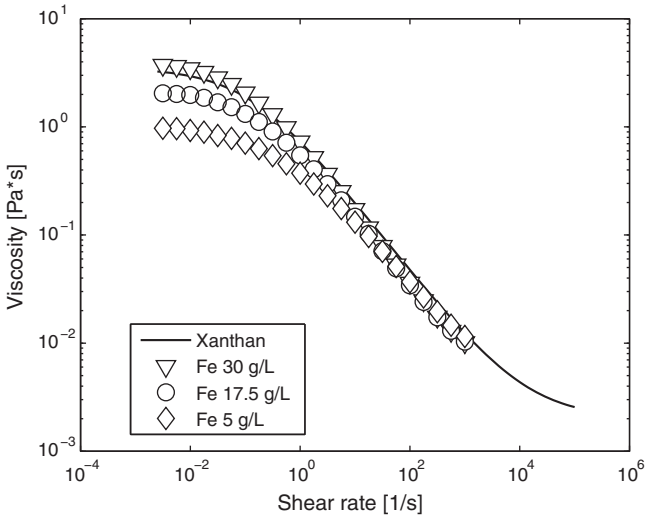

Fig. 3. Viscosity of NZVI-xanthan suspensions as a function of the shear rate. Since a replication was performed for every sample, the results were reported as the average of the two experiments.

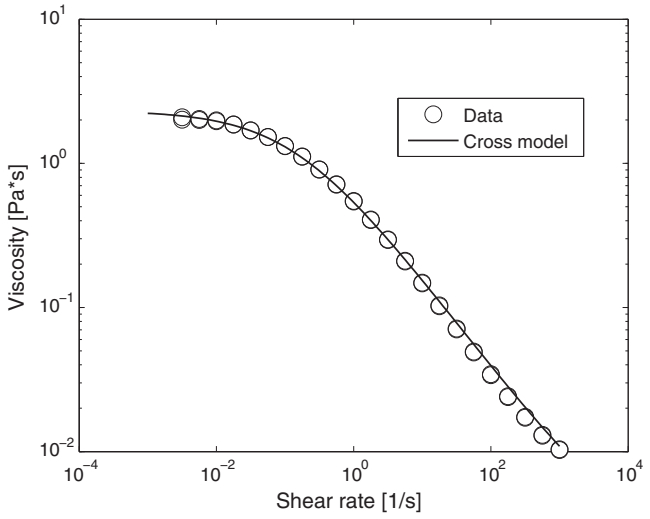

Fig. 4. Simple shear viscosity of 5 g l^{-1} NZVI suspensions as a function of the shear rate: experimental data (symbols) and fitted with the cross equation (solid line).

an increase in the iron concentration is associated to a higher shear rate viscosity and to more pronounced shear thinning behaviour.

3.2.2. Apparent viscosity determined from column tests

The results of the tests for evaluating the apparent rheology in porous medium are reported as viscosity versus shear rate curves (Fig. 5). Each set of viscosity and shear rate values was obtained from a column test, where discharge and stabilized pressure drop were measured. Therefore, the viscosity and shear rate were calculated using Eqs. (1) and (2), as described before.

Results pertaining to the xanthan solution are reported in Fig. 5. A shift factor α equal to 1 was applied to obtain the superposition between the simple shear and the apparent viscosity determined by column tests. This value which falls within the 1–15 range, is compatible with literature data, as reported in [35–37]. The shift factor depends on the tortuosity of the intergranular channels, and takes into account the greater distance which fluid must travel when crossing an intergranular channel than if it were to pass through a straight one. The low value of α obtained in this work indicates that the porous media structure is not very complex. This is consistent with the kind of porous medium used, which is a granular material with a relatively narrow grain size distribution.

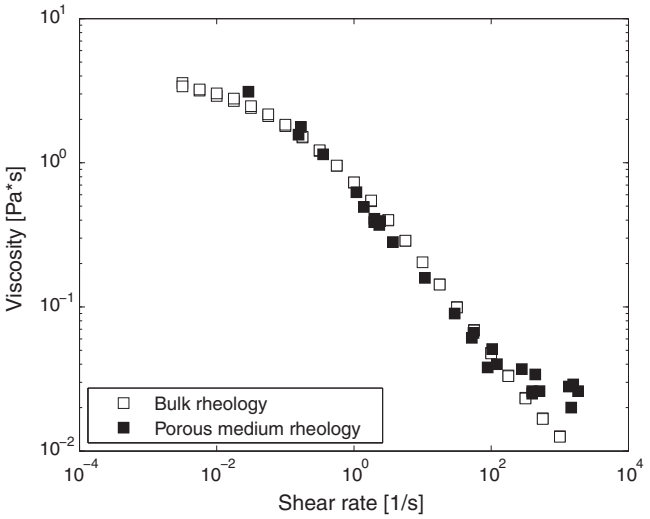

Fig. 5. Bulk rheology and apparent rheology in porous mediumfor 3 g l^{-1} xanthan solutions.

Results also indicate that shear dominates at low velocities, whereas the extensional nature of the flow induces an increase in the apparent viscosity after a specific strain rate, which is about 200 s^{-1}. Elongational flow, which is due to the change in the cross-section, influences apparent viscosity because both the macromolecules and their transient entanglements present residual flexibility [31].

Fig. 6 shows the friction factor as a function of the Reynolds number [49]:

$$f = \frac{\Delta P}{q^2}\frac{d_{10}}{L}\rho\frac{n^3}{1-n}$$

$$Re = \frac{d_{10}q}{\mu}\frac{1}{1-n}$$

where ΔP is the pressure drop, ρ is the density, d_{10} is the diameter of the 10 percentile grain size of the material, n is the porosity, q is specific discharge and L is the length of the porous medium. Since the Reynolds number is below or very close to 1, the creep-

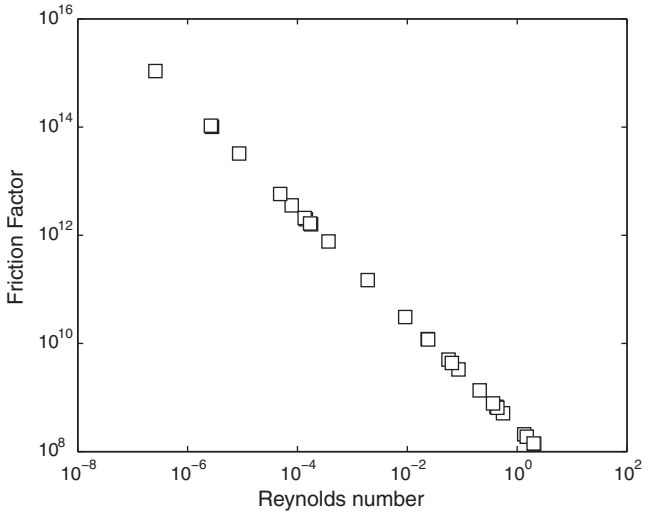

Fig. 6. Dimensionless pressure drop against Reynolds number for 3 g l^{-1} xanthan solutions.

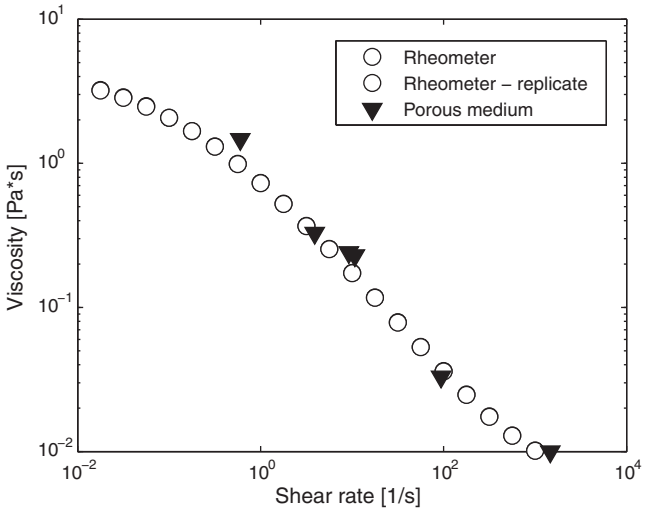

Fig. 7. Bulk rheology and apparent rheology in porous mediumfor suspensions with 30 g l^{-1} iron and 3 g l^{-1} xanthan.

ing flow occurs under the experimental conditions [50,51]. The same test was performed for the iron suspension, indicating again creeping flow conditions. The same test was performed for the iron suspension, indicating again creeping flow conditions.

Results of the experiments in a porous medium for the 30 g l^{-1} NZVI-xanthan solutions are reported in Fig. 7. A shift factor α equal to 1 was applied to obtain the superposition between the simple shear and the rheological behavior of solutions during their flow through the porous medium.

The behaviour observed in the porous media experiments greatly resembles that found in the rheometric flow experiments: the shear thinning and zero-shear viscosity increase with increasing iron concentration and the viscosity decreases when small amounts of iron particles are present. However, in porous media experiments, the viscosities of highly concentrated iron suspensions appear to be more similar to that of a xanthan fluid.

4. Discussion

In the injection test, a high quantity of iron particles was recovered at the column outlet. If the breakthrough results are compared with those from literature [8–12,14,17,19] it can be seen that an addition of 0.3 wt% of xanthan greatly enhances the delivery of nanoiron particles through porous media as was also proved in Ref. [21] for a shorter 1D system.

The injection test also verifies the feasibility of testing the rheological properties in porous media, since the suspension does not change significantly when passing through a granular system.

Rheological behavior was then carefully evaluated. According to [20] an iron-xanthan suspension can be modeled as shown in Fig. 8. The microstructure of the suspension therefore has two principal elements: the backbonenetwork, composed of xanthan polymer, and a small amount of iron particles (0.4% in volume) which are separated and spaced.

The shape of the $\mu(\dot{\gamma})$ curve for NZVI-xanthan suspensions is actually very similar to that of the xanthan solution. Therefore, the suspending medium rheology plays an important role on the overall iron suspension rheology (in both rheological and porous medium tests). This means that, from a rheological point of view, the backbone network of xanthan polymer [20] transmits the applied stresses throughout the gel network [52]. On the other hand, the presence of iron particles also influence the rheology, by causing a decrease in the zero-shear viscosity μ_0, compared to the viscosity of the xanthan solution. The zero shear viscosity, μ_0, represents the maximum resistance to flow shown by the suspension just before its initial structure is broken down. In the case of xanthan solutions, this resistance of the material is due to the property of dissolved xanthan molecules to form aggregates through hydrogen bonding and polymer entanglement [30]. It is likely that when iron particles are present, they interfere with the formation of the bonds, by occupying voids that would otherwise be available for bonding between the polymers. Therefore, iron particles weaken the gel structure.

In the NZVI-xanthan suspensions, the increase in the iron concentration corresponds to an increase in the zero-shear viscosity μ_0. The dependence of the viscosity on the particle concentration is common [52–55]. It is also intuitive that as the fraction of solids in the system rises, the amount of mass per unit volume of fluid also increases as does the energy required to move the fluid. The increase in the zero-shear viscosity μ_0, with increasing iron concentrations, is probably also a consequence of particle interaction; as the particles become more closely packed together, their attractive interaction becomes stronger, it becomes more difficult for particles to move freely, and resistance to flow (viscosity) increases. The existence of an attractive force between two NZVI particles embedded in xanthan gel has been demonstrated experimentally by [20].

Therefore, particles act in two opposite ways on rheology: on one hand they weaken the xanthan backbone structure and therefore decrease viscosity, on the other hand they determine an increase in viscosity as they become sufficiently concentrated.

This interpretation is supported by the decrease, with increasing iron concentrations, in both the onset of the shear rate pertaining to the shear thinning phenomenon (λ) and the viscosity dependence on shear thinning (m), in both measurement conditions. This increase in shear thinning means that the structure of the material is actually damaged by the presence of increasing iron amounts, as the bindings between the xanthan polymers are disrupted at progressively lower shear rates.

5. Implications for field use

The method of delivering iron particles to porous media is usually site-specific and is dependent on the type of geology as well as

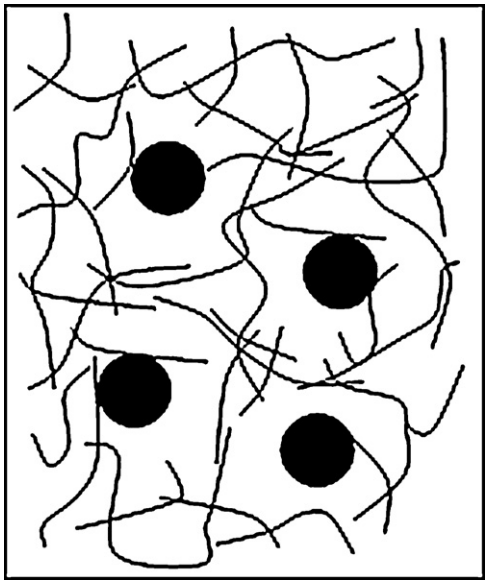

Fig. 8. Gelling xanthan polymer in NZVI colloidal dispersions: xanthan generates a network, to which particles can be either adsorbed or not. The picture is taken from [11].

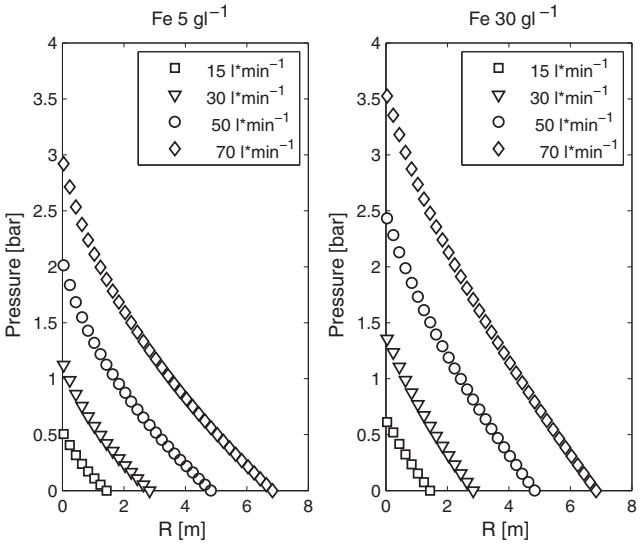

Fig. 9. Pressure field around the well for various radius of injection (ROI) and flow rate values.

particle dimensions. In permeable porous media and for nanoparticles, delivery can be achieved by means of permeation grouting techniques (i.e. gravity injection and pressurized injection), which simply involve filling the natural intergranular voids of the porous medium. On the contrary, in geologic formations with lower permeability and for micro and millimetric iron particles, the soil must be fractured by means of methods such as liquid atomization injection, pneumatic fracturing, hydraulic fracturing or soil mixing [56].

A simplified model has been developed in order to evaluate the feasibility of permeation grouting for injecting nanoscale-xanthan suspensions into porous medium.

The flow field around an injection well is typically radial. If the injection discharge is constant after reaching steady state conditions, velocity decreases hyperbolically with the distance from the well. The analytical expression of pressure P_{inj} at the injection point in the case of constant injection discharge and steady state conditions for a Newtonian fluid is well known:

$$P = P_{inj} - \frac{Q\mu}{2\pi hk} \ln \frac{R}{r_{inj}} \quad (4)$$

where P is the pressure at the distance R from the injection well, r_{inj} is the radius of the injection well, Q is the constant discharge, μ is the fluid viscosity, h is the height of the well screen and k is the permeability of the porous medium. In the case of injections under the water table, $P(R) = \dot{\gamma}_w \cdot z$, where z is the depth of the injection valve from the water table.

In the case of a shear thinning fluid, pressure cannot be calculated with Eq. (4) since the velocity, and therefore the viscosity of the material, changes with an increase in the distance from the well. However, the pressure at the injection point can be found numerically by discretizing the domain and evaluating Eq. (4) from the radius of influence of the injection (ROI) onwards to the well proximity, through the following equation:

$$P_{i+1} = P_i + \frac{Q\mu_i}{2\pi hk} \ln \frac{r_i}{r_{i+1}} \quad (5)$$

where i denotes the cell nearest to the radius of influence of the injection, while $i+1$ is the neighboring cell in the direction of the well. Viscosity can be calculated across the domain using the Cross equation, where the shear rate is calculated using Eq. (2).

The pressure field was calculated assuming that the suspensions were injected into an aquifer with properties similar to the porous medium used in this study and through a screening length of 0.33 m. The flow rate was varied between 15 and 70 l min^{-1}. The radius of influence of the injection (ROI) was defined as the distance from the well at which the velocity is equal to 1 cm min^{-1} and its value ranged from approximately 1.5 to 7 m.

As shown in Fig. 9, pressure gradually decays to zero as the distance from the well increases. The injection of iron suspensions should require pressures at the well between 1 and 3.5 bar, depending on the flow rate.

This range is suitable for field applications since piston pumps (Geoprobe) used with direct push systems are able to provide a flow rate of up to 30 l min^{-1} at 45 bar, while pressurized injection with inflatable packers are commonly performed at 10 l min^{-1} and at approximately 30 bar. Moreover the pressure values do not exceed the hydro-fracturing limit [57].

From Fig. 9, it is also clear that increasing the iron loadings would make the injection more difficult.

In conclusion, the use of xanthan suspensions to stabilize NZVI appears to be suitable when it is possible to achieve high shear rates during injection. When this condition is not possible, for example during gravity fed injection [58] xanthan modified suspensions appear to be less suitable.

6. Conclusions

The main findings and conclusions are as follows:

1. Simple shear rheology can be used as an estimate of the rheological behavior of solutions during their flow through the porous medium.
2. Xanthan gum is able to deliver iron particles through a sandy porous medium.
3. Iron-xanthan suspensions behave like non Newtonian shear thinning fluids, in a similar way to the dispersion medium. This is due to the microstructure of the suspension, where a backbone of xanthan polymer transmits the applied stresses through the gel network.
4. The presence of iron particles influences rheology. On one hand, by occupying sites that would otherwise be available for polymer bonding, iron particles weaken the xanthan structure, determining a zero shear viscosity decrease and more pronounced shear thinning behavior. On the other hand the predominant phenomenon at higher particle concentrations is the increase in zero shear viscosity, due to the particle attractive potential of interaction and to an increase in mass per unit volume.
5. The xanthan-NZVI suspensions can be used in the field, since the injection pressures are not excessively high. Natural transport by groundwater is expected to be only of minor importance in delivering iron particles. However, dilution due to groundwater could modify rheology and therefore the behavior in the aquifer after injection needs to be further investigated.

Appendix A.

A	cross-sectional area (m)
d	grain size diameter (m)
k	absolute permeability (m^2)
K	hydraulic conductivity (m s^{-1})
L	column length (m)
m	exponential parameter in the Cross model
n_e	effective porosity
Q	volumetric flow rate (m^3 s^{-1})
ΔP	pressure drop experienced along the column (Pa)
P	pressure at a distance x from the injection point (Pa)
P_{inj}	pressure at the injection point (Pa)

P_i pressure i of the cell nearest to the ROI (Pa)
P_{i+1} pressure of the cell nearest to the well (Pa)
q Darcy velocity ($m\,s^{-1}$)
s_w the specific weight of the liquid
$v = Q/(A\,n_e)$ average frontal velocity in the porous medium ($m\,s^{-1}$)
α constant factor used to obtain the superposition simple shear and porous medium superposition
$\dot{\gamma}$ shear rate (s^{-1})
μ shear viscosity (Pa s)
μ_{app} apparent or in situ viscosity (Pa s)
μ_0 asymptotic values of viscosity at low shear rates in the Cross model (Pa s)
μ_∞ asymptotic values of viscosity at high shear rates in the Cross model (Pa s)
λ parameter in the Cross model related to the shear rate value where shear thinning starts (s).

References

[1] M.J. Alowitz, M.M. Scherer, Kinetics of nitrate, nitrite, and Cr(VI) reduction by iron metal, Environmental Science & Technology 36 (2002) 299–306.
[2] J Dries, L. Bastiaens, D. Springael, S. Kuypers, S.N. Agathos, L. Diels, Effect of humic acids on heavy metal removal by zero-valent iron in batch and continuous flow column systems, Water Research 39 (2005) 3531–3540.
[3] R. Lookman, L. Bastiaens, B. Borremans, M. Maesen, J. Gemoets, L. Diels, Batch-test study on the dechlorination of 1,1,1-trichloroethane in contaminated aquifer material by zero-valent iron, Journal of Contaminant Hydrology 74 (2004) 133–144.
[4] R. Miehr, P.G. Tratnyek, J.Z. Bandstra, M.M. Scherer, M.J. Alowitz, E.J. Bylaska, Diversity of contaminant reduction reactions by zerovalent iron: role of the reductate, Environmental Science & Technology 38 (2003) 139–147.
[5] P.G. Tratnyek, M.M. Scherer, B. Deng, S. Hu, Effects of natural organic matter, anthropogenic surfactants, and model quinones on the reduction of contaminants by zero-valent iron, Water Research 35 (2001) 4435–4443.
[6] A Di Molfetta, R. Sethi, Clamshell excavation of a permeable reactive barrier, Environmental Geology 50 (2006) 361–369.
[7] P.G. Tratnyek, R.L. Johnson, Nanotechnologies for environmental cleanup, Nano Today 1 (2006) 44–48.
[8] B. Schrick, B.W. Hydutsky, J.L. Blough, T.E. Mallouk, Delivery vehicles for zerovalent metal nanoparticles in soil and groundwater, Chemistry of Materials 16 (2004) 2187–2193.
[9] S.R. Kanel, D. Nepal, B. Manning, H. Choi, Transport of surface-modified iron nanoparticle in porous media and application to arsenic(III) remediation, Journal of Nanoparticle Research 9 (2007) 725–735.
[10] G.C.C. Yang, H.C. Tu, C.H. Hung, Stability of nanoiron slurries and their transport in the subsurface environment, Separation and Purification Technology 58 (2007) 166–172.
[11] N. Saleh, T. Phenrat, K. Sirk, B. Dufour, J. Ok, T. Sarbu, K. Matyiaszewski, R.D. Tilton, G.V. Lowry, Adsorbed triblock copolymers deliver reactive iron nanoparticles to the oil/water interface, Nano Letters 5 (2005) 2489–2494.
[12] N. Saleh, K. Sirk, Y.Q. Liu, T. Phenrat, B. Dufour, K. Matyjaszewski, R.D. Tilton, G.V. Lowry, Surface modifications enhance nanoiron transport and NAPL targeting in saturated porous media, Environmental Engineering Science 24 (2007) 45–57.
[13] Y.P. Sun, X.Q. Li, W.X. Zhang, H.P. Wang, A method for the preparation of stable dispersion of zero-valent iron nanoparticles, Colloids and Surfaces A-Physicochemical and Engineering Aspects 308 (2007) 60–66.
[14] A. Tiraferri, K.L. Chen, R. Sethi, M. Elimelech, Reduced aggregation and sedimentation of zero-valent iron nanoparticles in the presence of guar gum, Journal of Colloid and Interface Science 324 (2008) 71–79.
[15] A. Tiraferri, R. Sethi, Enhanced transport of zerovalent iron nanoparticles in saturated porous media by guar gum, Journal of Nanoparticle Research 11 (2009) 635–645.
[16] F. He, D.Y. Zhao, Manipulating the size and dispersibility of zerovalent iron nanoparticles by use of carboxymethyl cellulose stabilizers, Environmental Science & Technology 41 (2007) 6216–6221.
[17] F. He, D.Y. Zhao, J.C. Liu, C.B. Roberts, Stabilization of Fe-Pd nanoparticles with sodium carboxymethyl cellulose for enhanced transport and dechlorination of trichloroethylene in soil and groundwater, Industrial and Engineering Chemistry Research 46 (2007) 29–34.
[18] F. He, D.Y. Zhao, Preparation and characterization of a new class of starch-stabilized bimetallic nanoparticles for degradation of chlorinated hydrocarbons in water, Environmental Science & Technology 39 (2005) 3314–3320.
[19] B.W. Hydutsky, E.J. Mack, B.B. Beckerman, J.M. Skluzacek, T.E. Mallouk, Optimization of nano- and microiron transport through sand columns using polyelectrolyte mixtures, Environmental Science & Technology 41 (2007) 6418–6424.
[20] S. Comba, R. Sethi, Stabilization of highly concentrated suspensions of iron nanoparticles using shear-thinning gels of xanthan gum, Water Research 43 (2009) 3717–3726.
[21] E. Dalla Vecchia, M. Luna, R. Sethi, Transport in porous media of highly concentrated iron micro- and nanoparticles in the presence of xanthan gum, Environmental Science & Technology 43 (2009) 8942–8947.
[22] M. Oostrom, T.W. Wietsma, M.A. Covert, V.R. Vermeul, Zero-valent iron emplacement in permeable porous media using polymer additions, Ground Water Monitoring and Remediation 27 (2007) 122–130.
[23] C.L. Perrin, P.M.J. Tardy, K.S. Sorbie, J.C. Crawshaw, Experimental and modeling study of Newtonian and non-Newtonian fluid flow in pore network micromodels, Journal of Colloid and Interface Science 295 (2006) 542–550.
[24] R. Martel, A. Hebert, R. Lefebvre, P. Gelinas, U. Gabriel, Displacement and sweep efficiencies in a DNAPL recovery test using micellar and polymer solutions injected in a five-spot pattern, Journal of Contaminant Hydrology 75 (2004) 1–29.
[25] K.E. Martel, R. Martel, R. Lefebvre, P.J. Gelinas, Laboratory study of polymer solutions used for mobility control during in situ NAPL recovery, Ground Water Monitoring and Remediation 18 (1998) 103–113.
[26] T. Robert, R. Martel, S.H. Conrad, R. Lefebvre, U. Gabriel, Visualization of TCE recovery mechanisms using surfactant-polymer solutions in a two-dimensional heterogeneous sand model, Journal of Contaminant Hydrology 86 (2006) 3–31.
[27] N.W.H. Cheetham, E.N.M. Mashimba, Characterization of some enzymatic-hydrolysis products of xanthan, Carbohydrate Polymers 15 (1991) 195–206.
[28] Y. Viturawong, P. Achayuthakan, M. Suphantharika, Gelatinization and rheological properties of rice starch/xanthan mixtures: effects of molecular weight of xanthan and different salts, Food Chemistry 111 (2008) 106–114.
[29] K.L. Chen, S.E. Mylon, M. Elimelech, Aggregation kinetics of alginate-coated hematite nanoparticles in monovalent and divalent electrolytes, Environmental Science & Technology 40 (2006) 1516–1523.
[30] Z.H. Mohammed, A. Haque, R.K. Richardson, E.R. Morris, Promotion and inhibition of xanthan 'weak-gel' rheology by calcium ions, Carbohydrate Polymers 70 (2007) 38–45.
[31] J.M. Gonzalez, A.J. Muller, M.F. Torres, A.E. Saez, The role of shear and elongation in the flow of solutions of semi-flexible polymers through porous media, Rheologica Acta 44 (2005) 396–405.
[32] R.P. Chhabra, J. Comiti, I. Machac, Flow of non-Newtonian fluids in fixed and fluidised beds, Chemical Engineering Science 56 (2001) 1–27.
[33] C.D. Tsakiroglou, A methodology for the derivation of non-Darcian models for the flow of generalized Newtonian fluids in porous media, Journal of Non-Newtonian Fluid Mechanics 105 (2002) 79–110.
[34] C.D. Tsakiroglou, Correlation of the two-phase flow coefficients of porous media with the rheology of shear-thinning fluids, Journal of Non-Newtonian Fluid Mechanics 117 (2004) 1–23.
[35] X. Lopez, P.H. Valvatne, M.J. Blunt, Predictive network modeling of single-phase non-Newtonian flow in porous media, Journal of Colloid and Interface Science 264 (2003) 256–265.
[36] G. Chauveteau, Rodlike polymer solution flow through fine pores: influence of pore size on rheological behavior, Journal of Rheology 26 (1982) 111–142.
[37] G. Chauveteau, Fundamental criteria in polymer flow through porous-media - and their importance in the performance differences of mobility-control buffers, Advances in Chemistry Series (1986) 227–267.
[38] K.S. Sorbie, Y.D. Huang, Rheological and transport effects in the flow of low-concentration xanthan solution through porous-media, Journal of Colloid and Interface Science 145 (1991) 74–89.
[39] J.R.A. Pearson, P.M.J. Tardy, Models for flow of non-Newtonian and complex fluids through porous media, Journal of Non-Newtonian Fluid Mechanics 102 (2002) 447–473.
[40] J.T. Nurmi, P.G. Tratnyek, V. Sarathy, D.R. Baer, J.E. Amonette, K. Pecher, C. Wang, J.C. Linehan, D.W. Matson, R.L. Penn, M.D. Driessen, Characterization and properties of metallic iron nanoparticles: spectroscopy, electrochemistry, and kinetics, Environmental Science and Technology 39 (2005) 1221–1230.
[41] G Philips, P. Williams, Handbook of Hydrocolloids, 2000.
[42] M.Z. Liu, R.S. Cheng, R.Y. Qian, Effects of solution concentration on the gelation of aqueous polyvinyl-alcohol solution, Journal of Polymer Science: Polymer Chemistry 33 (1995) 1731–1735.
[43] B. Launay, Rheological aspects of the gelling of bioproducts, Biofutur (1997) A9–A11.
[44] C. Macosko, Rheology: Principles, Measurements, and Applications, VCH Publishers, 1995.
[45] A.S. Dukhin, P.J. Goetz, Bulk viscosity and compressibility measurement using acoustic spectroscopy, The Journal of Chemical Physics 130 (2009) 124519.
[46] M. Cross, Rheology of non-Newtonian fluids: a new flow equation for pseudoplastic systems, Journal of Colloid Science 20 (1965) 417–437.
[47] R. Saggin, J.N. Coupland, Rheology of xanthan/sucrose mixtures at ultrasonic frequencies, Journal of Food Engineering 65 (2004) 49–53.
[48] P.J. Whitcomb, B.J. Ek, C.W. Macosko, Rheology of xanthan gum solutions, in: Extracellular Microbial Polysaccharides, American Chemical Society, Washington, DC, 1977, pp. 160–173.
[49] R.B. Bird, W.E. Stewart, E.N. Lightfoot, Transport Phenomena, Wiley, 1960.
[50] J. Bear, Dynamics of Fluids in Porous Media, Dover Publications, New York, 1972.
[51] R.B. Bird, W.E. Stewart, E.N. Lightfoot, Transport Phenomena, Wiley, 2002.
[52] S. Peker, S. Helvaci, Solid–Liquid Two Phase Flow, 2007.
[53] P. Coussot, Rheometry of Pastes, Suspensions, and Granular Materials, 1st ed., Wiley-Interscience, Hoboken, 2005.

[54] L. Bergstrom, Shear thinning and shear thickening of concentrated ceramic suspensions, Colloids and Surfaces A-Physicochemical and Engineering Aspects 133 (1998) 151–155.
[55] C.M. Vladu, C. Hall, G.C. Maitland, Flow properties of freshly prepared ettringite suspensions in water at LE 25 degrees C, Journal of Colloid and Interface Science 294 (2006) 466–472.
[56] S. Comba, A. Di Molfetta, R. Sethi, A comparison between field applications of nano, micro and millimetric zero-valent iron for the remediation of contaminated aquifers, Water, Air and Soil Pollution (2010).
[57] C. Kutzner, Grouting of Rock and Soil, Rotterdam, 1996.
[58] D.W. Elliott, W.-x. Zhang, Field assessment of nanoscale bimetallic particles for groundwater treatment, Environmental Science & Technology 35 (2001) 4922–4926.